A Series of Novel Mercury(I) Selenites and Tellurites Containing SOJT Mo^{6+} Cations

Xue-Li Cao, Fang Kong, Chun-Li Hu, and Jiang-Gao Mao*

Supporting Information

Table S1. IR data for Hg_2MoSeO_6, β-Hg_2MoTeO_6 and $Hg_2Mo_2TeO_9$.

	ν(Mo-O)	ν(Te(Se)-O)	ν(Mo-O-Te(Se))
Hg_2MoSeO_6	926, 919, 852, 799	710	565, 514, 476, 434
β-Hg_2MoTeO_6	902, 890, 835, 802	772, 743, 670	630, 488, 432
$Hg_2Mo_2TeO_9$	916, 865, 838	719, 651	580, 538, 465

Table S2. The state energies (eV) of the lowest conduction band (L-CB) and the highest valence band (H-VB) of four compounds

Compound	k-point	L-CB	H-VB
Hg_2MoSeO_6	G (0.000, 0.000, 0.000)	2.37967	-0.22391
	Z (0.000, 0.000, 0.500)	2.09588	-0.22611
	T (-0.500, 0.000, 0.500)	2.05515	-0.0151
	Y (-0.500, 0.000, 0.000)	2.00846	-0.22226
	S (-0.500, 0.500, 0.000)	2.10684	-0.20726
	X (0.000, 0.500, 0.000)	2.41997	-0.3026
	U (0.000, 0.500, 0.500)	2.10284	-0.24112
	R (-0.500, 0.500, 0.500)	2.05513	-0.08394
α-Hg_2MoTeO_6	G (0.000, 0.000, 0.000)	2.23388	-0.17412
	Z (0.000, 0.000, 0.500)	1.90561	-0.22908
	T (-0.500, 0.000, 0.500)	1.95669	-0.01492
	Y (-0.500, 0.000, 0.000)	1.97193	-0.12817
	S (-0.500, 0.500, 0.000)	2.07563	-0.11001
	X (0.000, 0.500, 0.000)	2.26734	-0.20701
	U (0.000, 0.500, 0.500)	1.9297	-0.25045
	R (-0.500, 0.500, 0.500)	1.95764	-0.0552
β-Hg_2MoTeO_6	G (0.000, 0.000, 0.000)	2.37232	0
	Z (0.000, 0.000, 0.500)	2.37061	-0.1893
	T (-0.500, 0.000, 0.500)	2.39828	-0.16734
	Y (-0.500, 0.000, 0.000)	2.39235	-0.10826
	S (-0.500, 0.500, 0.000)	2.45	-0.30942
	X (0.000, 0.500, 0.000)	2.42851	-0.17048
	U (0.000, 0.500, 0.500)	2.45738	-0.24798
	R (-0.500, 0.500, 0.500)	2.46164	-0.36117
$Hg_2Mo_2TeO_9$	Z (0.000, 0.000, 0.500)	1.94429	-0.38463
	G (0.000, 0.000, 0.000)	1.95989	-0.31202
	Y (0.000, 0.500, 0.000)	1.95281	-0.40158
	A (-0.500, 0.500, 0.000)	2.00094	-0.2354
	B (-0.500, 0.000, 0.000)	1.92089	0
	D (-0.500, 0.000, 0.500)	1.95858	-0.15148
	E (-0.500, 0.500, 0.500)	1.9605	-0.23011
	C (0.000, 0.500, 0.500)	1.94002	-0.44692

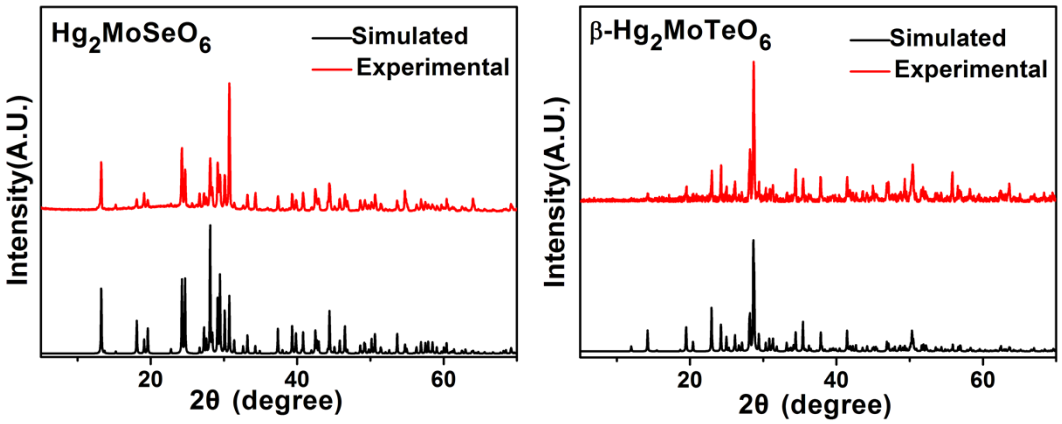

(a)

(b)

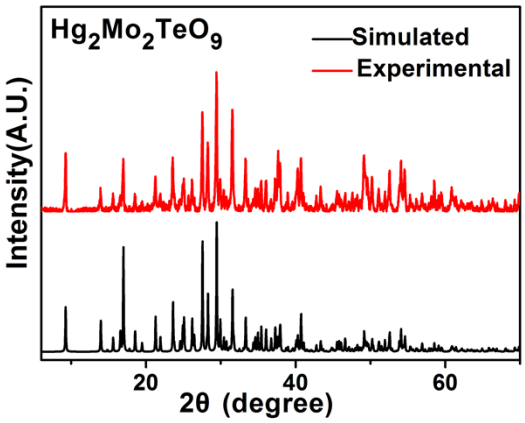

(c)

Figure S1. Simulated and experimental XRD powder patterns of Hg_2MoSeO_6 (a), *β*-Hg_2MoTeO_6 (b) and $Hg_2Mo_2TeO_9$ (c).

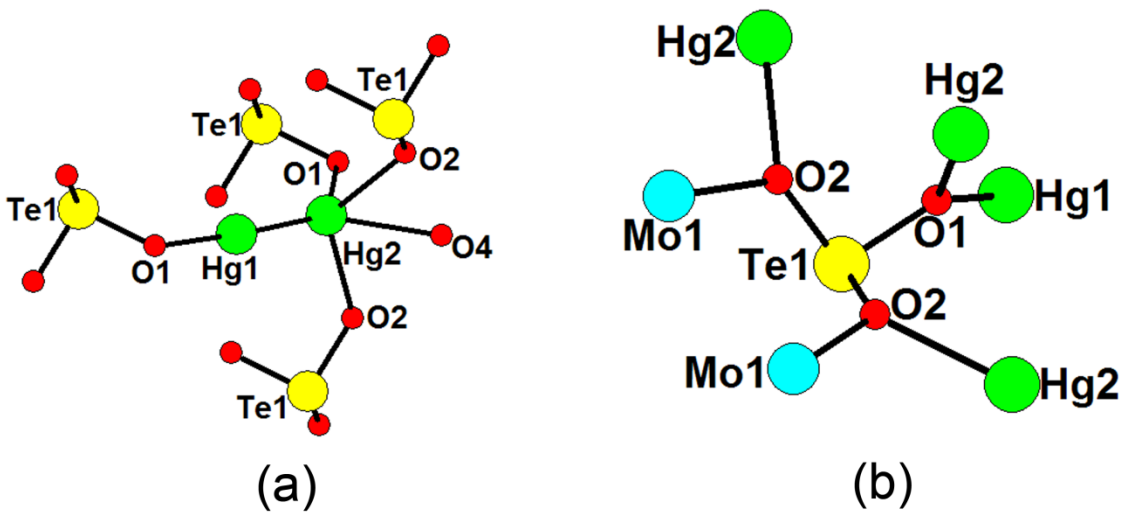

Figure S2. The coordination environment around the Hg^{+} cation (a) and the coordination mode of the tellurite group (b) in α-Hg_2MoTeO_6.

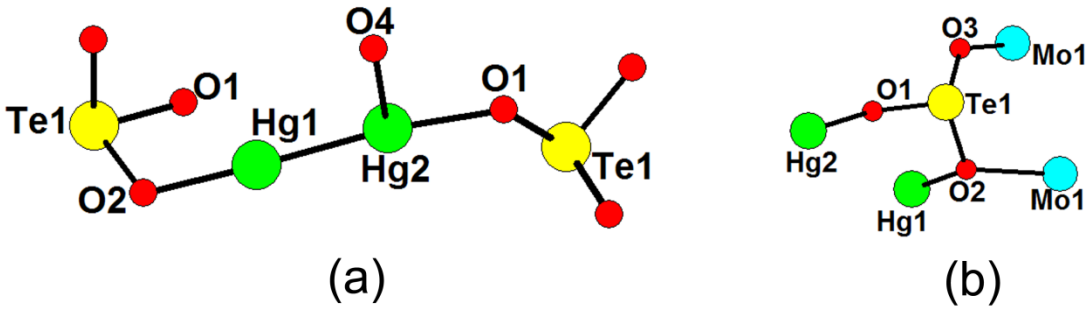

Figure S3. The coordination geometries around Hg^{+} cations (a) and the coordination mode of the tellurite group (b) in β-Hg_2MoTeO_6.

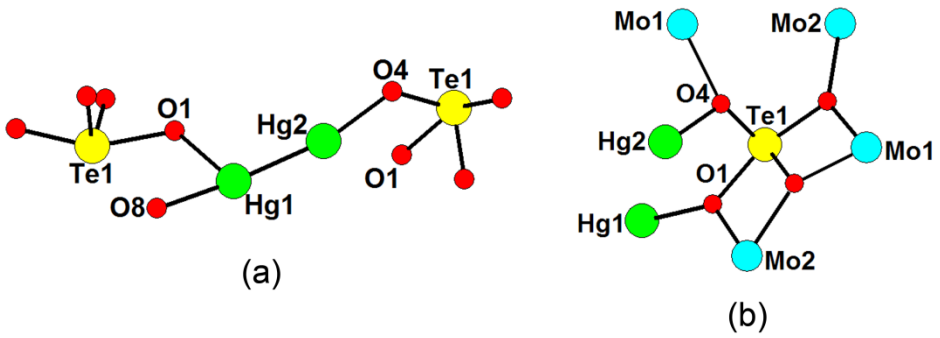

Figure S4. The coordination geometries around Hg^{+} cations (a) and the coordination mode of the tellurite group (b) in $Hg_2Mo_2TeO_9$.

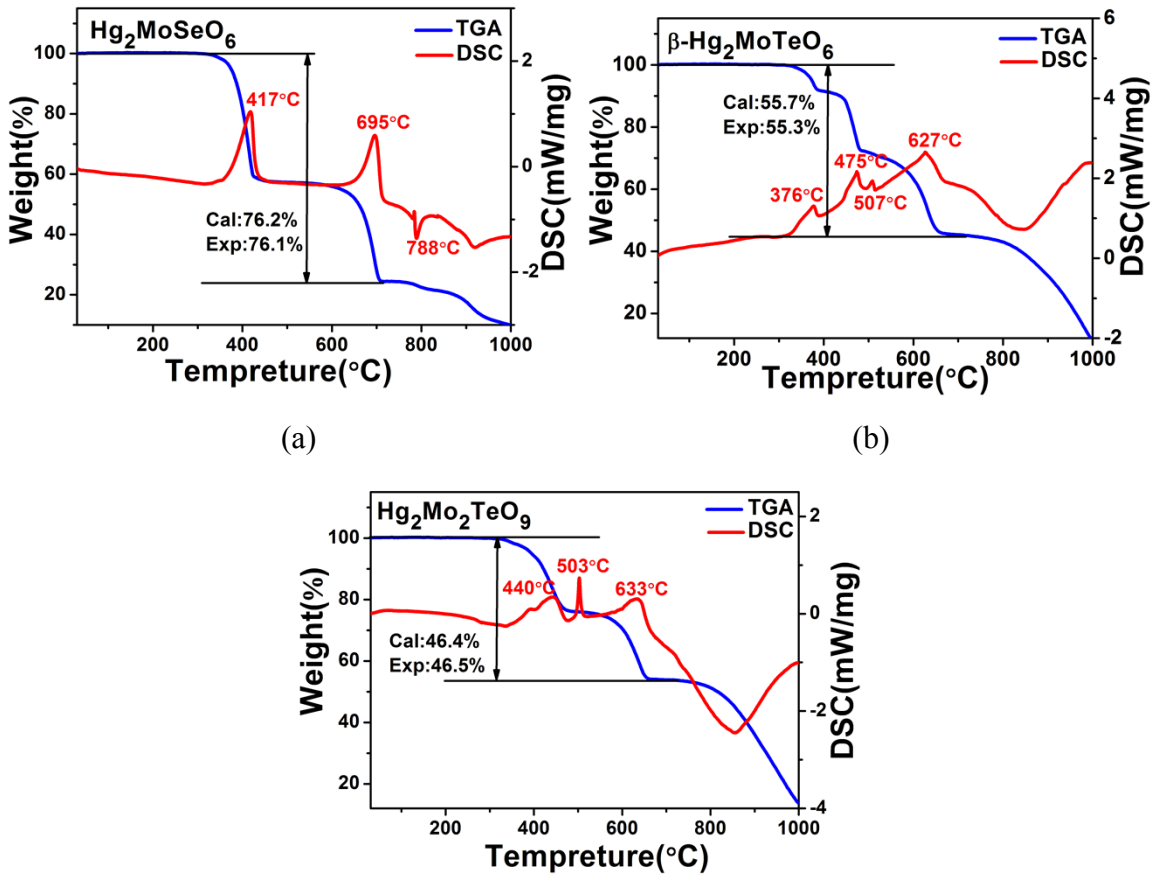

Figure S5. TGA and DSC curves of Hg_2MoSeO_6 (a), β-Hg_2MoTeO_6 (b) and $Hg_2Mo_2TeO_9$ (c).

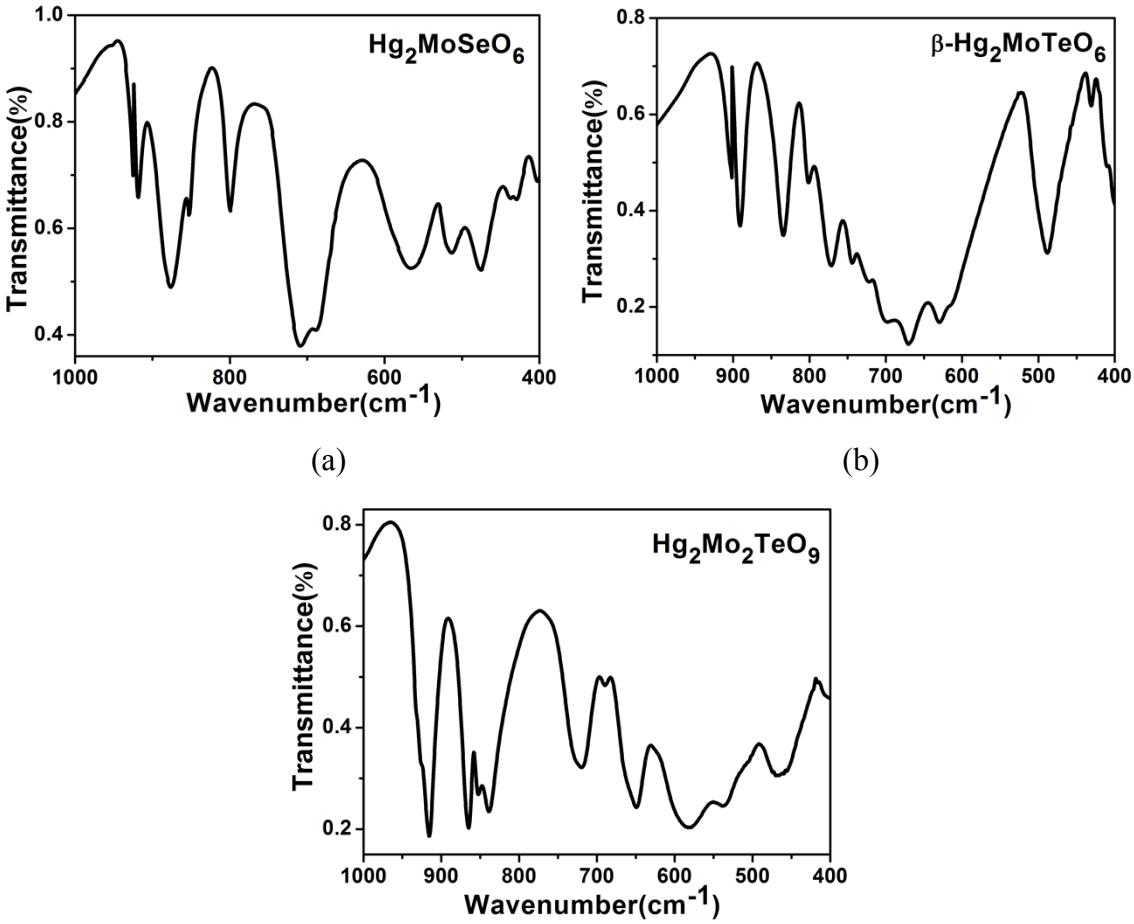

Figure S6. IR spectra of Hg_2MoSeO_6 (a), *β*-Hg_2MoTeO_6 (b) and $Hg_2Mo_2TeO_9$ (c).

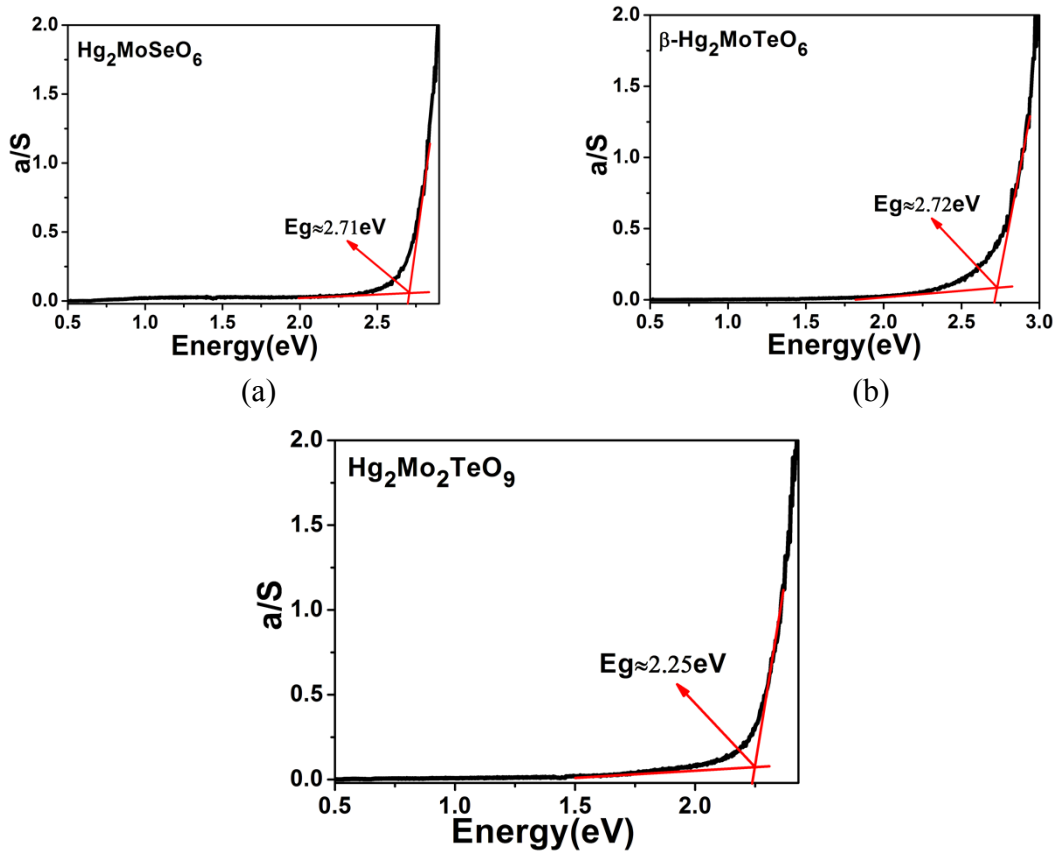

Figure S7. Optical diffuse reflectance spectra of Hg_2MoSeO_6 (a), β-Hg_2MoTeO_6 (b) and $Hg_2Mo_2TeO_9$ (c).